

REASON: Accelerating Probabilistic Logical Reasoning for Scalable Neuro-Symbolic Intelligence

Zishen Wan[†], Che-Kai Liu, Jiayi Qian, Hanchen Yang, Arijit Raychowdhury, Tushar Krishna

School of Electrical and Computer Engineering, Georgia Institute of Technology, Atlanta, GA

{zishenwan, che-kai, jiayiqian, hanchen}@gatech.edu, {arijit.raychowdhury, tushar}@ece.gatech.edu

Abstract—Neuro-symbolic AI systems integrate neural perception with symbolic and probabilistic reasoning to enable data-efficient, interpretable, and robust intelligence beyond purely neural models. Although this compositional paradigm has shown superior performance in domains such as mathematical reasoning, planning, and verification, its deployment remains challenging due to severe inefficiencies in symbolic and probabilistic inference. Through systematic analysis of representative neuro-symbolic workloads, we identify probabilistic logical reasoning as the inefficiency bottleneck, characterized by irregular control flow, low arithmetic intensity, uncoalesced memory accesses, and poor hardware utilization on CPUs and GPUs.

This paper presents REASON, an integrated acceleration framework for probabilistic logical reasoning in neuro-symbolic AI. At the algorithm level, REASON introduces a unified directed acyclic graph representation that captures common structure across symbolic and probabilistic models, coupled with adaptive pruning and regularization. At the architecture level, REASON features a reconfigurable, tree-based processing fabric optimized for irregular traversal, symbolic deduction, and probabilistic aggregation. At the system level, REASON is tightly integrated with GPU streaming multiprocessors through a programmable interface and multi-level pipeline that efficiently orchestrates neural, symbolic, and probabilistic execution. Evaluated across six neuro-symbolic workloads, REASON achieves $12\text{-}50\times$ speedup and $310\text{-}681\times$ energy efficiency over desktop and edge GPUs under TSMC 28 nm node. REASON enables real-time probabilistic logical reasoning, completing end-to-end tasks in 0.8 s with 6 mm² area and 2.12 W power, demonstrating that targeted acceleration of probabilistic logical reasoning is critical for practical and scalable neuro-symbolic AI and positioning REASON as a foundational system architecture for next-generation cognitive intelligence.

I. INTRODUCTION

Large Language Models (LLMs) have demonstrated remarkable capabilities in natural language understanding, image recognition, and complex pattern learning from vast datasets [1]–[4]. However, despite their success, LLMs often struggle with factual accuracy, hallucinations, multi-step reasoning, and interpretability [5]–[8]. These limitations have spurred the development of *compositional AI systems*, which integrate neural with symbolic and probabilistic reasoning to create robust, transparent, and intelligent cognitive systems.

One promising compositional paradigm is neuro-symbolic AI, which integrates neural, symbolic, and probabilistic components into a unified cognitive architecture [9]–[13]. In this system, the *neural* module captures the statistical, pattern-matching behavior of learned models, performing rapid function approximation and token prediction for intuitive percep-

tion and feature extraction. The *symbolic* and *probabilistic* modules perform explicit, verifiable reasoning that is structured, interpretable, and robust under uncertainty, managing logic-based reasoning and probabilistic updates. This paradigm integrates intuitive generalization and deliberate reasoning.

Neuro-symbolic AI has demonstrated superior abstract deduction, complex question answering, mathematical reasoning, logical reasoning, and cognitive robotics [14]–[21]. Its ability to learn efficiently from fewer data points, produce transparent and verifiable outputs, and robustly handle uncertainty and ambiguity makes it particularly advantageous compared to purely neural approaches. For example, recently Meta’s LIPS [14] and Google’s AlphaGeometry [15] leverage compositional neuro-symbolic approaches to solve complex math problems and achieve a level of human Olympiad gold medalists. R²-Guard [22] leverages LLM and probabilistic models to improve robust reasoning capability and resilience against jailbreaks. They represent a paradigm shift for AI that requires robust, verifiable, and explainable reasoning.

Despite impressive algorithmic advances in neuro-symbolic AI – often demonstrated on large-scale distributed GPU clusters – efficient deployment at the edge remains a fundamental challenge. Neuro-symbolic agents, particularly in robotics, planning, interactive cognition, and verification, require *real-time* logical inference to interact effectively with physical environments and multi-agent systems. For example, Ctrl-G, a text-infilling neuro-symbolic agent [23], must execute hundreds of reasoning steps per second to remain responsive, yet current implementations take over 5 minutes on a desktop GPU to complete a single task. This latency gap makes practical deployment of neuro-symbolic AI systems challenging.

To understand the root causes of this inefficiency, we systematically analyze a diverse set of neuro-symbolic workloads and uncover several system- and architecture-level challenges. Symbolic and probabilistic kernels frequently dominate end-to-end runtime and exhibit highly irregular execution characteristics, including heterogeneous compute patterns and memory-bound behavior with low ALU utilization. These kernels suffer from limited exploitable parallelism and irregular, uncoalesced memory accesses, leading to poor performance and efficiency on CPU and GPU architectures.

To address these challenges, we develop an integrated acceleration framework, REASON, which to the best of our knowledge, is the first to accelerate probabilistic logical reasoning-based neuro-symbolic AI systems. REASON is designed to

[†]Corresponding author

close the efficiency gap of compositional AI by jointly optimizing algorithms, architecture, and system integration for the irregular and heterogeneous workloads inherent to neuro-symbolic reasoning.

At the algorithm level, REASON introduces a unified directed acyclic graph (DAG) representation that captures shared computational structure across symbolic and probabilistic kernels. An adaptive pruning and regularization technique further reduces model size and computational complexity while preserving task accuracy. At the architecture level, REASON features a flexible design optimized for various irregular symbolic and probabilistic computations, leveraging the unified DAG representation. The architecture comprises reconfigurable tree-based processing elements (PEs), compiler-driven workload mapping, and memory layout to enable highly parallel and energy-efficient symbolic and probabilistic computation. At the system level, REASON is tightly integrated with GPU streaming multiprocessors (SMs), forming a heterogeneous system with a programmable interface and multi-level execution pipeline that efficiently orchestrates neural, symbolic, and probabilistic kernels while maintaining high hardware utilization and scalability as neuro-symbolic models evolve. Notably, unlike conventional tree-like computing arrays optimized primarily for neural workloads, REASON provides reconfigurable support for neural, symbolic, and probabilistic kernels within a unified execution fabric, enabling efficient and scalable neuro-symbolic AI systems.

This paper, therefore, makes the following contributions:

- We conduct a systematic workload characterization of representative logical- and probabilistic-reasoning-based neuro-symbolic AI models, identifying key performance bottlenecks and architectural optimization opportunities (Sec. II, Sec. III).
- We propose REASON, an integrated co-design framework, to efficiently accelerate probabilistic logical reasoning in neuro-symbolic AI, enabling practical and scalable deployment of compositional intelligence (Fig. 4).
- REASON introduces cross-layer innovations spanning (i) a unified DAG representation with adaptive pruning at the algorithm level (Sec. IV), (ii) a reconfigurable symbolic/probabilistic architecture and compiler-driven dataflow and mapping at the hardware level (Sec. V), and (iii) a programmable system interface with a multi-level execution pipeline at the system level (Sec. VI) to improve neuro-symbolic efficiency.
- Evaluated across cognitive tasks, REASON enables flexible support for symbolic and probabilistic operations, achieving $12\text{-}50\times$ speedup and $310\text{-}681\times$ energy efficiency compared to desktop and edge GPUs. REASON enables fast and efficient logical and probabilistic reasoning in 0.8 s per task with 6 mm² area and 2.12 W power consumption. (Sec. VII).

II. NEURO-SYMBOLIC AI SYSTEMS

This section presents the preliminaries of neuro-symbolic AI with its algorithm flow (Sec. II-A), scaling performance anal-

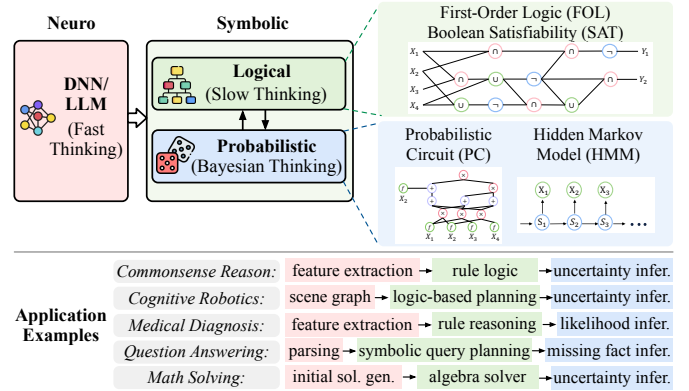


Fig. 1: Neuro-symbolic algorithmic flow and operations. The neural module serves as a perceptual and intuitive engine for representation learning, while the symbolic module performs structured logical reasoning with probabilistic inference. This compositional pipeline enables complex cognitive tasks across diverse scenarios.

ysis (Sec. II-B), and key computational primitives (Sec. II-C).

A. Neuro-Symbolic Cognitive Intelligence

LLMs and DNNs excel at natural language understanding and image recognition. However, they remain prone to factual errors, hallucinations, challenges in complex multi-step reasoning, and vulnerability to out-of-distribution or adversarial inputs. Their black-box nature also impedes interpretability and formal verification, undermining trust in safety-critical domains. These limitations motivate the development of *compositional* systems that integrate neural models with symbolic and probabilistic reasoning to achieve greater robustness, transparency, and intelligence.

Neuro-symbolic AI represents a paradigm shift toward more integrated and trustworthy intelligence by combining neural, symbolic, and probabilistic techniques. This hybrid approach has shown superior performance in abstract deduction [17], [18], complex question answering [19], [20], and logical reasoning [15], [16]. By learning from limited data and producing transparent, verifiable outputs, neuro-symbolic systems provide a foundation for cognitive intelligence. Fig. 1 presents a unified neuro-symbolic pipeline, illustrating how its components collaborate to solve complex tasks.

Neural module. The neural module serves as the perceptual and intuitive engine, typically DNN or LLM, excelling at processing high-dimensional sensory inputs (e.g., images, audio, text) and converting them into feature representations. It handles perception, feature extraction, and associative learning, providing the abstractions needed for higher-level cognition.

Symbolic module. The symbolic module is the logical core operating on neural abstractions and includes symbolic and probabilistic operations. *Logical* components apply formal logic, rules, and ontologies for structured reasoning and planning, enabling logically sound solutions. *Probabilistic* components manage uncertainty by representing knowledge probabilistically, supporting belief updates and decision-making under ambiguity, reflecting a nuanced reasoning model.

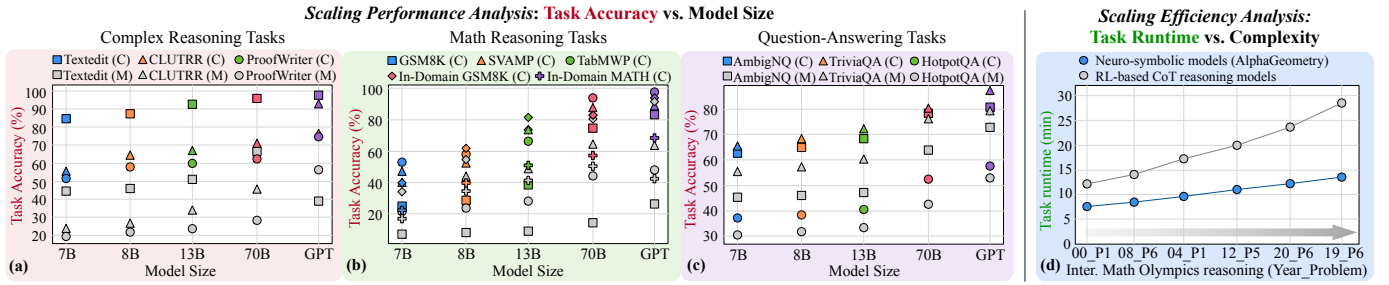


Fig. 2: Scaling performance and efficiency. (a)-(c) Task accuracy of compositional LLM-symbolic models (C) and monolithic LLMs (M - shown in gray) across model sizes on complex reasoning, mathematical reasoning, and question-answering tasks. (d) Runtime efficiency comparison between LLM-symbolic models and RL-based CoT models on mathematical reasoning tasks [24].

Together, these modules form a complementary reasoning hierarchy. Neural module captures statistical, pattern-matching behavior of learned models, producing rapid but non-verifiable outputs (*Fast Thinking*), while symbolic modules perform explicit, verifiable reasoning that is structured and reliable (*Slow Thinking*). The probabilistic module complements both and enables robust planning under ambiguity (*Bayesian Thinking*). This framework integrates intuitive generalization with deliberate reasoning.

B. Scaling Performance Analysis of Neuro-Symbolic Systems

Scaling performance analysis. Neuro-symbolic AI systems exhibit superior reasoning capability and scaling behavior compared to monolithic LLMs on complex tasks. We compare representative neuro-symbolic systems against monolithic LLMs across complex reasoning, mathematical reasoning, and question-answering benchmarks (Fig. 2(a)-(c)). The results reveal two advantages. *First, higher accuracy:* compositional neuro-symbolic models consistently outperform monolithic LLMs of comparable size. *Second, improved scaling efficiency:* smaller neuro-symbolic models are sufficient to match or exceed the performance of significantly larger closed-source LLMs. Together, these results highlight the potential scaling limitations of monolithic LLMs and the efficiency benefits of compositional neuro-symbolic reasoning.

Comparison with RL-based reasoning models. Beyond monolithic LLMs, recent advancements in reinforcement learning (RL) and chain-of-thought (CoT) prompting improve LLM reasoning accuracy but incur significant computational and scalability overheads (Fig. 2(d)). *First, computational cost:* RL-based reasoning often requires hundreds to thousands of LLM queries per decision step, resulting in prohibitively high inference latency and energy consumption. *Second, scalability:* task-specific fine-tuning constrains generality, whereas neuro-symbolic models use symbolic and probabilistic reasoning modules or tools without retraining. Fig. 2(d) reveals that neuro-symbolic models AlphaGeometry [15] achieve over 2× efficiency gains and superior data efficiency compared to CoT-based LLMs on mathematical reasoning tasks.

C. Computational Primitives in Neuro-Symbolic AI

We identify the core computational primitives that are commonly used in neuro-symbolic AI systems (Fig. 1). While neu-

ral modules rely on DNNs or LLMs for perception and representation learning, the symbolic and probabilistic components implement structured reasoning. In particular, *logical reasoning* is typically realized through First-Order Logic (FOL) and Boolean Satisfiability (SAT), *probabilistic reasoning* through Probabilistic Circuits (PCs), and *sequential reasoning* through Hidden Markov Models (HMMs). Together, these primitives form the algorithmic foundation of neuro-symbolic systems that integrate learning, logic, and uncertainty-aware inference.

First-Order Logic (FOL) and Boolean Satisfiability (SAT). FOL provides a formal symbolic language for representing structured knowledge using predicates, functions, constants, variables and quantifiers (\forall, \exists), combined with logical connectives. For instance, the statement “every student has a mentor” can be expressed as $\forall x(\text{Student}(x) \rightarrow \exists y(\text{Mentor}(y) \wedge \text{hasMentor}(x, y)))$, where predicates encode properties and relations over domain elements. FOL semantics map symbols to domain objects and relations, enabling precise and interpretable logical reasoning. SAT operates over propositional logic and asks whether a conjunctive normal form (CNF) formula $\varphi = \bigwedge_{i=1}^m \left(\bigvee_{j=1}^{k_i} l_{ij} \right)$ admits a satisfying assignment, where each literal l_{ij} is a Boolean variable or its negation. Modern SAT solvers extend the DPLL algorithm with conflict-driven clause learning (CDCL), incorporating non-chronological backtracking and clause learning to improve scalability [25], [26]. Cube-and-conquer further parallelizes search by splitting into “cube” DPLL subproblems and concurrent CDCL “conquer” solvers [27], [28]. Together, FOL’s expressive representations and SAT’s solving mechanisms form the logic backbone of neuro-symbolic systems, enabling exact logical inference alongside neural learning.

Probabilistic Circuits (PC). PCs represent tractable probabilistic models over variables \mathbf{X} as directed acyclic graphs [32]–[34]. Each node n performs a probabilistic computation: leaf nodes specify primitive distributions $f_n(x)$, while interior nodes combine their children $ch(n)$ via

$$p_n(x) = \begin{cases} f_n(x), & \text{if } n \text{ is a leaf node} \\ \prod_{c \in ch(n)} p_c(x), & \text{if } n \text{ is a product node} \\ \sum_{c \in ch(n)} \theta_{n,c} p_c(x), & \text{if } n \text{ is a sum node} \end{cases} \quad (1)$$

where $\theta_{n,c}$ denotes the non-negative weight associated with child c . This recursive structure guarantees exact inference

Representative Neuro-Symbolic Workloads		AlphaGeometry [15]	R ² -Guard [22]	GeLaTo [29]	Ctrl-G [23]	NeuroPC [30]	LINC [31]
Deployment Scenario	Application	Math theorem proving & reasoning	Unsafety detection	Constrained text generation	Interactive text editing, text infilling	Classification	Logical reasoning, Deductive reasoning
	Advantage vs. LLM	Higher deductive reasoning, higher generalization	Higher LLM resilience, higher data efficiency, effective adaptability	Guaranteed constraint satisfaction, higher generalization	Guaranteed constraints satisfaction, higher generalization	Enhanced interpretability, theoretical guarantee	Higher precision, reduced overconfidence, higher scalability
Computation Pattern	Neural	LLM	LLM	LLM	LLM	DNN	LLM
	Symbolic	First-order logic, SAT solver, probabilistic circuit, Hidden Markov model	First-order logic, SAT solver, Hidden Markov model	First-order logic, SAT solver, Hidden Markov model	Hidden Markov model, probabilistic circuits	First-order logic, probabilistic circuit	First-order logic, solver

TABLE I: Representative neuro-symbolic workloads. Selected neuro-symbolic workloads used in our analysis, spanning diverse application domains, deployment scenarios, and neural-symbolic computation patterns.

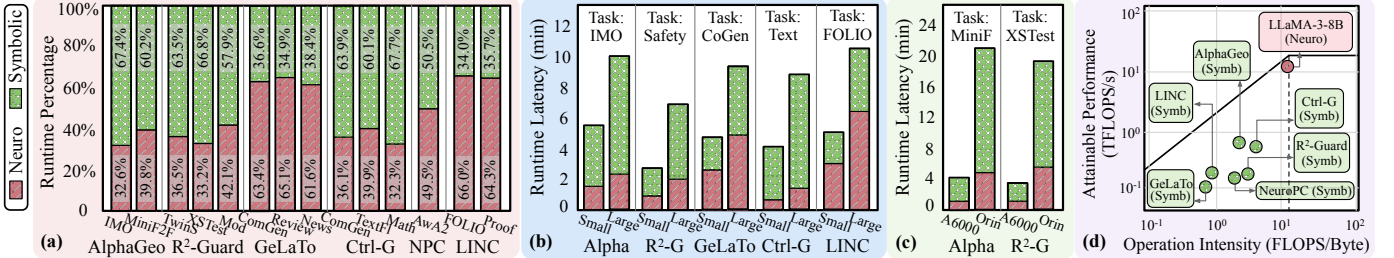


Fig. 3: End-to-end neuro-symbolic workload characterization. (a) Benchmark six neuro-symbolic workloads (AlphaGeometry, R²-Guard, GeLaTo, Ctrl-G, NeuroPC, LINC) on CPU+GPU system, showing symbolic and probabilistic may serve as system bottlenecks. (b) Benchmark neuro-symbolic workloads on tasks with different scales, indicating that real-time performance cannot be satisfied and the potential efficiency issues. (c) Benchmark on A6000 and Orin GPU. (d) Roofline analysis, indicating server memory-bound of symbolic and probabilistic kernels.

(e.g., marginals, conditionals) in time linear in circuit size. PCs' combination of expressiveness and tractable computation makes them an ideal probabilistic backbone for neuro-symbolic systems, where neural modules learn circuit parameters while symbolic engines perform probabilistic reasoning.

Hidden Markov Model (HMM). HMMs are probabilistic model for sequential data [35], where a system evolves through hidden states governed by the first-order Markov property: the state at time step t depends only on the state at time step $t - 1$. Each hidden state emits observations according to a probabilistic distribution. The joint distribution over sequence of hidden states $z_{1:T}$ and observations $x_{1:T}$ is given by

$$p(z_{1:T}, x_{1:T}) = p(z_1)p(x_1 | z_1) \prod_{t=2}^T p(z_t | z_{t-1})p(x_t | z_t) \quad (2)$$

where $p(z_1)$ is the initial state distribution, $p(z_t | z_{t-1})$ the transition probability, and $p(x_t | z_t)$ the emission probability. HMMs naturally support sequential inference tasks such as filtering, smoothing, and decoding, enabling temporal reasoning in neuro-symbolic pipelines.

III. NEURO-SYMBOLIC WORKLOAD CHARACTERIZATION

This section characterizes the system behavior of various neuro-symbolic workloads (Sec. III-A-III-B) and provides workload insights for computer architects (Sec. III-C-III-D).

Profiling workloads. To conduct comprehensive profiling analysis, we select six state-of-the-art representative neuro-symbolic workloads, as listed in Tab. I, covering a diverse range of applications and underlying computational patterns.

Profiling setup. We profile and analyze the selected neuro-symbolic models in terms of runtime, memory, and com-

pute operators using cProfile for latency measurement, and NVIDIA Nsight for kernel-level profiling and analysis. Experiments are conducted on the system with NVIDIA A6000 GPU, Intel Sapphire Rapids CPUs, and DDR5 DRAM. Our software environment includes PyTorch 2.5 and JAX 0.4.6. We also conduct profiling on Jetson Orin [36] for edge scenario deployment. We track control and data flow by analyzing the profiling results in trace view and graph execution format.

A. Compute Latency Analysis

Latency bottleneck. We characterize the latency of representative neuro-symbolic workloads (Fig. 3(a)). *Compared to neuro kernels, symbolic and probabilistic kernels are not negligible in latency and may become system bottlenecks.* For instance, the neural (symbolic) components account for 36.2% (63.8%), 37.3% (62.7%), 63.4% (36.6%), 36.1% (63.9%), 49.5% (50.5%), and 65.2% (34.8%) of runtime in AlphaGeometry, R²-Guard, GeLaTo, Ctrl-G, NeuroPC, and LINC, respectively. Symbolic kernels dominate AlphaGeometry's runtime, and probabilistic kernels dominate R²-Guard and Ctrl-G's, due to high irregular memory access, wrap divergence, thread underutilization, and execution parallelism. FLOPS and latency measurements further highlight this inefficiency. Notably, when using a smaller LLM (LLaMA-7B) for GeLaTo and LINC, overall accuracy remains stable, but the symbolic latency rises to 69.0% and 65.5%, respectively. We observe consistent trends in the Orin NX-based platform (Fig. 3(c)). Symbolic components count for 63.8% of AlphaGeometry runtime on A6000 while its FLOPS count for only 19.3%, indicating inefficient hardware utilization.

Latency scalability. We evaluate runtime across reasoning tasks of varying difficulty and scale (Fig. 3(b)). We observe

TABLE II: Hardware inefficiency analysis. The compute, memory, and communication characteristics of representative neural, symbolic, and probabilistic kernels executed on CPU/GPU platform.

	Neural Kernel		Symbolic Kernel		Probabilistic Kernel	
	MatMul	Softmax	Sparse MatVec	Logic	Marginal	Bayesian
<i>Compute Efficiency</i>						
Compute Throughput (%)	96.8	62.2	32.5	14.7	35.0	31.1
ALU Utilization (%)	98.4	72.0	43.9	29.3	48.5	52.8
<i>Memory Behavior</i>						
L1 Cache Throughput (%)	82.4	58.0	27.1	20.6	32.4	37.1
L2 Cache Throughput (%)	41.7	27.6	18.3	12.4	24.2	27.5
L1 Cache Hit Rate (%)	88.5	85.0	53.6	37.0	42.4	40.7
L2 Cache Hit Rate (%)	73.4	66.7	43.9	32.7	50.2	47.6
DRAM BW Utilization (%)	39.8	28.6	57.4	70.3	60.8	68.0
<i>Control Divergence and Scheduling</i>						
Warp Execution Efficiency (%)	96.3	94.1	48.8	54.0	59.3	50.6
Branch Efficiency (%)	98.0	98.7	60.0	58.1	63.4	66.9
Eligible Warps/Cycle (%)	7.2	7.0	2.4	2.1	2.8	2.5

that the relative runtime distribution between neural and symbolic components remains consistent of a single workload across task sizes. Total runtime increases with task complexity and scale. While LLM kernels scale efficiently due to their tensor-based GPU-friendly inference, logical and probabilistic kernels scale poorly due to the exponential growth of search space, making them slower compared to monolithic LLMs.

B. Roofline & Symbolic Operation & Inefficiency Analysis

Memory-bounded operation. Fig. 3(d) presents a roofline analysis of GPU memory bandwidth versus compute efficiency. We observe that the symbolic and probabilistic components are typically memory-bound, limiting performance efficiency. For example, R²-Guard’s probabilistic circuits use sparse, scattered accesses for marginalization, and Ctrl-G’s HMM iteratively reads and writes state probabilities. Low compute per element makes these workloads constrained by memory access, underutilizing GPU compute resources.

Hardware inefficiency analysis. We leverage Nsight Systems and Nsight Compute [37], [38] to analyze the computational, memory, and control irregularity of neural, symbolic, and probabilistic kernels, as listed in Tab. II. We observe that: *First, compute throughput and ALU utilization*: neural kernels achieve high throughput and ALU utilization, while symbolic/probabilistic kernels have low throughput and idle ALUs. *Second, memory access and cache utilization*: neural kernels see high L1 cache hit rates; symbolic kernels incur cache

misses and stalls, and probabilistic kernels face high memory pressure. *Third, DRAM bandwidth (BW) utilization and data movement overhead*: neural workloads use on-chip caches with minimal DRAM usage, but symbolic/probabilistic workloads are DRAM-bound with heavy random-access overhead.

Sparsity analysis. We observe high, heterogeneous, irregular, and data-dependent sparsity across neuro-symbolic workloads. Symbolic and probabilistic kernels are often extremely sparse, exhibiting on average 82%, 87%, 75%, 83%, 89%, and 83% sparsity across six representative neuro-symbolic workloads, respectively, with many sparse computational paths based on low activation or probability mass. This observation motivates our *adaptive DAG pruning* (Sec IV-B).

C. Unique Characteristics of Neuro-Symbolic vs LLMs

In summary, neuro-symbolic workloads exhibit distinct characteristics compared to monolithic LLMs in compute kernels, memory behavior, dataflow, and performance scaling.

Compute kernels. LLMs are dominated by regular, highly parallel tensor operations well suited to GPUs. In contrast, neuro-symbolic workloads comprise heterogeneous symbolic and probabilistic kernels with irregular control flow, low arithmetic intensity, and poor cache locality, leading to low GPU utilization and frequent performance bottlenecks.

Memory behavior. Symbolic and probabilistic kernels are primarily memory-bound, operating over large, sparse, and irregular data structures. Probabilistic reasoning further increases memory pressure through large intermediate state caching, creating challenging trade-offs between latency, bandwidth, and on-chip storage.

Dataflow and parallelism. Neuro-symbolic workloads exhibit dynamic and tightly coupled data dependencies. Symbolic and probabilistic computations often depend on neural outputs or require compilation into LLM-compatible structures, resulting in serialized execution, limited parallelism, and amplified end-to-end latency.

Performance scaling. LLMs scale efficiently across GPUs via optimized data and model parallelism. In contrast, symbolic workloads are difficult to parallelize due to recursive control dependencies, while probabilistic kernels incur substantial inter-node communication, limiting scalability on multi-GPUs.

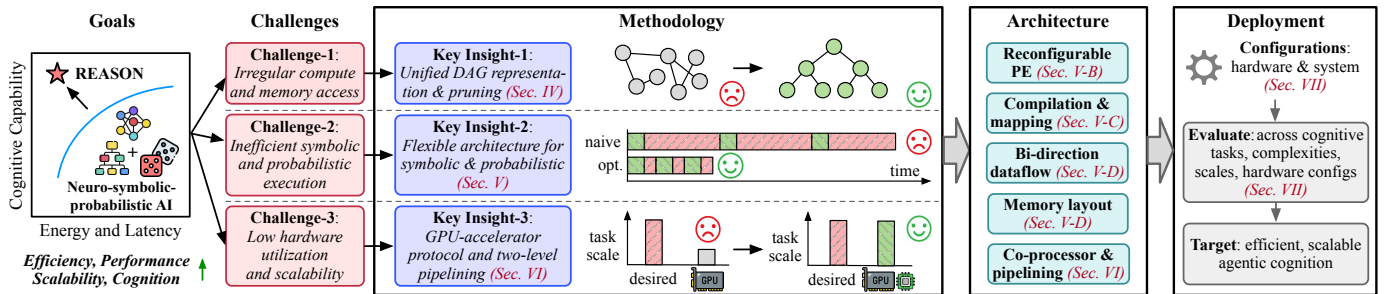


Fig. 4: REASON overview. REASON is an integrated acceleration framework for probabilistic logical reasoning grounded neuro-symbolic AI with the goal to achieve efficient and scalable agentic cognition. REASON addresses the challenges of irregular compute and memory, symbolic and probabilistic latency bottleneck, and hardware underutilization, by proposing methodologies including unified DAG representation, reconfigurable PE, efficient dataflow, mapping, scalable architecture, two-level parallelism and programming interface. REASON is deployed across cognitive tasks and consistently demonstrates performance-efficiency improvements for compositional neuro-symbolic systems.

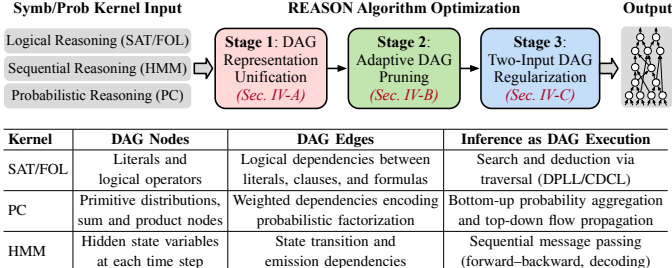


Fig. 5: Unified DAG representations of neuro-symbolic kernels. Logical (SAT/FOL), probabilistic (PC), and sequential (HMM) reasoning are expressed using DAG abstraction. Nodes represent atomic reasoning operations, edges encode dependency structure, and graph traversals implement inference procedures. This unification enables shared compilation, pruning, and hardware mapping in REASON.

D. Identified Opportunities for Neuro-Symbolic Optimization

While neuro-symbolic systems show promise, improving their efficiency is critical for real-time and scalable deployment. Guided by the profiling insights above, we introduce REASON (Fig. 4), an algorithm-hardware co-design framework for accelerated probabilistic logical reasoning in neuro-symbolic AI. Algorithmically, a unified representation with adaptive pruning reduces memory footprint (Sec. IV). In hardware architecture, a flexible architecture and dataflow support various symbolic and probabilistic operations (Sec. V). REASON further provides adaptive scheduling and orchestration of heterogeneous LLM-symbolic agentic workloads through a programmable interface (Sec. VI). Across reasoning tasks, REASON consistently boosts performance, efficiency, and accuracy (Sec. VII).

IV. REASON: ALGORITHM OPTIMIZATIONS

This section introduces the algorithmic optimizations in REASON for symbolic and probabilistic reasoning kernels. We present a unified DAG-based computational representation (Sec. IV-A), followed by adaptive pruning (Sec. IV-B) and regularization techniques (Sec. IV-C) that jointly reduce model complexity and enable efficient neuro-symbolic systems.

A. Stage 1: DAG Representation Unification

Motivation. Despite addressing different reasoning goals, symbolic and probabilistic reasoning kernels often share common underlying computational patterns. For instance, logical deduction in FOL, constraint propagation in SAT, and marginal inference in PCs all rely on iterative graph-based computations. Capturing this shared structure is essential to system acceleration. DAGs provide a natural abstraction to unify these diverse kernels under a flexible computational model.

Methodology. We unify symbolic and probabilistic reasoning kernels under a DAG abstraction, where each node represents an atomic reasoning operation and each directed edge encodes a data/control dependency (Fig. 5). This representation enables a uniform compilation flow – construction, transformation, and scheduling – across heterogeneous kernels (logical deduction, constraint solving, probabilistic aggregation, and

sequential message passing), and serves as the algorithmic substrate for subsequent pruning and regularization.

a) For FOL and SAT solvers: DAG nodes represent variables and logical connectives, with edges indicating dependencies between literals and clauses. We represent a propositional CNF formula $\varphi = \bigwedge_{i=1}^m \left(\bigvee_{j=1}^{k_i} l_{ij} \right)$ as DAG with three layers: literal nodes for each literal l_{ij} , clause nodes implementing disjunction over literals in $\bigvee_j l_{ij}$, and formula nodes implementing conjunction over clauses \bigwedge_i . In SAT, DAG captures the branching and conflict resolution structures in DPLL/CDCL procedures. In FOL, formulas are encoded as DAGs where inference rules act as graph transformation operators that derive contradictions through node and edge expansion. The compiler converts FOL and SAT inputs (clauses in CNF or quantifier-free predicates) into DAGs via: *Step-1* **Normalization:** predicates are transformed to CNF, removing quantifiers and forming disjunctions of literals. *Step-2* **Node creation:** each literal becomes a leaf node, each clause an OR node over its literals, and the formula an AND node over clauses. *Step-3* **Edge encoding:** edges capture dependencies (literal \rightarrow clause \rightarrow formula), while watch-lists as metadata.

b) For PCs: DAG nodes correspond to sum (mixture) or product (factorization) operations $p_n(x)$ over input x (to variable \mathbf{X}), with children $ch(x)$. Leaves represent primitive distributions $f_n(x)$. Edges model conditional dependencies. The DAG structure facilitates efficient inference through bottom-up probability evaluation, exploiting structural independence and enabling effective pruning and memorization during probability queries (Eq. 1). The compiler converts PC into DAGs through: *Step-1* **Graph extraction:** nodes represent random variables, factors, or sub-circuits parsed from expressions such as $P_n(x)$. *Step-2* **Node typing:** arithmetic operators map to sum nodes for marginalization and product nodes for factor conjunction, while leaf nodes store constants or probabilities.

c) For HMMs: The unrolled DAG spans time steps, with nodes representing transition factors $p(z_t|z_{t-1})$ and emission factors $p(x_t|z_t)$ (Eq. 2), and edges connecting factors across adjacent time steps to reflect Markov dependency. Sequential inference (filtering/smoothing/decoding) becomes structured message passing on this DAG: each step aggregates contributions from predecessor states through transition factors and then applies emission factors. The compiler converts HMMs into DAGs through: *Step-1* **Sequence unroll:** Each time step becomes a DAG layer, representing states and transitions. *Step-2* **Node mapping:** Product nodes combine transition and emission probabilities; sum nodes aggregate over prior states.

The unified DAG abstraction lays the algorithmic foundation for subsequent pruning, regularization, and hardware mapping, supporting efficient acceleration of neuro-symbolic workloads.

B. Stage 2: Adaptive DAG Pruning

Motivation. While the unified DAG representation provides a common abstraction, it may contain significant redundancy, such as logically implied literals, inactive substructures, or low-probability paths, that inflate DAG size and degrade performance without improving inference quality.

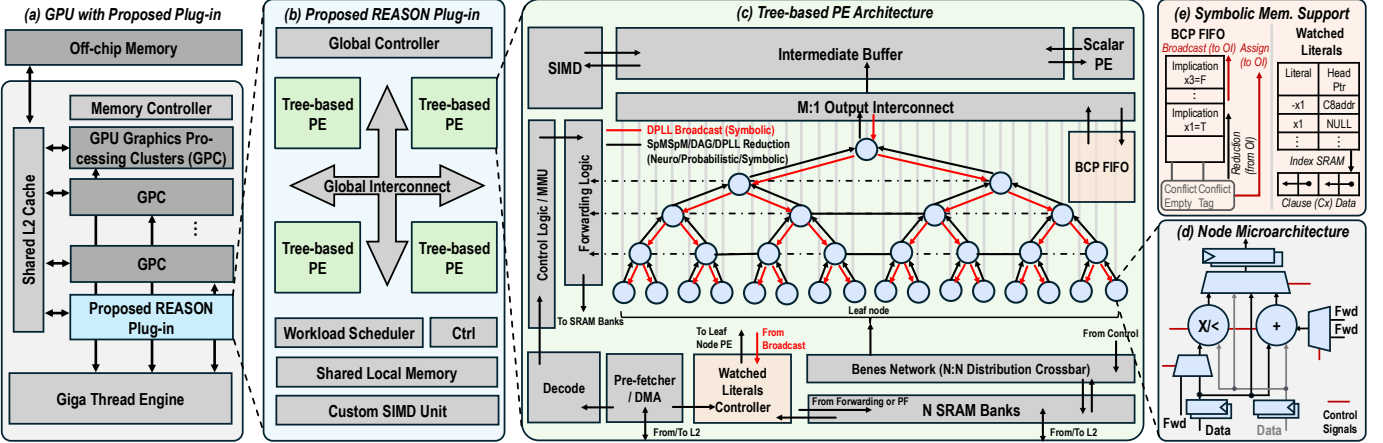


Fig. 6: Overview of the REASON hardware acceleration system. (a) Integration of REASON as a GPU co-processor. (b) REASON plug-in architecture with PEs, shared local memory, and global scheduling. (c) Tree-based PE architecture enabling broadcast, reduction, and irregular DAG execution. (d) Micro-architecture of a tree node supporting arithmetic and logical operations. (e) FIFO and memory layout supporting symbolic reasoning.

Methodology. We propose adaptive DAG pruning, a semantics-preserving optimization that identifies and removes redundant paths in symbolic and probabilistic DAGs. For symbolic kernels, pruning targets literals and clauses that are logically redundant. For probabilistic kernels, pruning eliminates low-activation edges that minimally impact inference. This process significantly reduces model size and computational complexity while preserving correctness of logical and probabilistic inference.

a) *Pruning of FOL and SAT via implication graph:* For SAT solvers and FOL reasoning, we prune redundant literals using implication graphs. Given a CNF formula $\varphi = \bigwedge_i (\bigvee_j l_{ij})$, each binary clause $(l \vee l')$ induces two directed implication edges: $\bar{l} \rightarrow l'$ and $\bar{l}' \rightarrow l$. The resulting implication graph captures logical dependencies among literals. We perform a depth-first traversal to compute reachability relationships between literals. If a literal l' is always implied by another literal l , then l' is a hidden literal. Clauses containing both l and l' can safely drop l' , reducing clause width without semantic changes. For instance, a clause $C = (l \vee l')$ is reduced to $C' = (l)$. This procedure removes redundant literals (e.g., hidden tautologies and failed literals), preserves satisfiability, and runs in time linear in the size of the implication graph.

b) *Pruning of PCs and HMMs via circuit flow:* For probabilistic DAGs such as PCs and HMMs, we prune edges based on probability flow, which quantifies each edge's contribution to the overall likelihood.

In HMMs, the DAG is unrolled over time steps, with nodes representing transition factors $p(z_t | z_{t-1})$ and emission factors $p(x_t | z_t)$. We compute expected transition and emission usage via the forward-backward algorithm, yielding posterior state and transition probabilities. Edges corresponding to transitions or emissions with consistently low posterior probability are pruned, as their contribution to the joint likelihood $p(z_{1:T}, x_{1:T})$ is negligible. This pruning preserves inference fidelity while reducing state-transition complexity.

In PCs, sum node n computes $p_n(x) = \sum_{c \in \text{ch}(n)} \theta_{n,c} p_c(x)$,

where $\theta_{n,c} \geq 0$ denotes the weight associated with child c . For an input x , we define the circuit flow through edge (n, c) as $F_{n,c}(x) = \frac{\theta_{n,c} p_c(x)}{p_n(x)} \cdot F_n(x)$, where $F_n(x)$ denotes the top-down flow reaching node n . Intuitively, $F_{n,c}(x)$ measures the fraction of probability mass passing through edge (n, c) for input x . Given a dataset \mathcal{D} , the cumulative flow for edge (n, c) is $F_{n,c}(\mathcal{D}) = \sum_{x \in \mathcal{D}} F_{n,c}(x)$. Edges with the smallest cumulative flow are pruned, as they contribute least to the overall model likelihood. The resulting decrease in average log-likelihood is bounded by $\Delta \log \mathcal{L} \leq \frac{1}{|\mathcal{D}|} \sum_{x \in \mathcal{D}} F_{n,c}(x)$, providing a theoretically grounded criterion for safe pruning.

C. Stage 3: Two-Input DAG Regularization

Methodology. After pruning, the resulting DAGs may still have high fan-in or irregular branching, which hinders efficient hardware execution. To address this, we apply a regularization step that transforms DAGs into a canonical two-input form. Specifically, nodes with more than two inputs are recursively decomposed into balanced binary trees composed of two-input intermediate nodes, preserving the original computation semantics. This normalization promotes uniformity, enabling efficient parallel scheduling, pipelining, and mapping onto REASON architecture, without sacrificing model fidelity or expressive power.

For each symbolic or probabilistic kernel, the compiler generates an initial DAG, applies adaptive pruning, and then performs two-input regularization to produce a unified balanced representation. These DAGs are constructed offline and used to generate an execution binary that is programmed onto REASON hardware. This unification-pruning-regularization flow decouples algorithmic complexity from runtime execution and enables predictable performance.

V. REASON: HARDWARE ARCHITECTURE

REASON features flexible co-processor plug-in architecture (Sec. V-A), reconfigurable symbolic/probabilistic PEs (Sec. V-B), flexible support for symbolic and probabilistic

kernels (Sec. V-C-V-D). Sec. V-E presents cycle-by-cycle execution pipeline analysis. Sec. V-F discusses design space exploration and scalability.

A. Overall Architecture

Neuro-symbolic workloads exhibit heterogeneous compute and memory patterns with diverse sparsity, diverging from the GEMM-centric design of conventional hardware. Built on the unified DAG representation and optimizations (Fig. IV), REASON is a reconfigurable and flexible architecture designed to efficiently execute the irregular computations of symbolic and probabilistic reasoning stages in neuro-symbolic AI.

Overview. REASON operates as a programmable co-processor tightly integrated with GPU SMs, forming a heterogeneous system architecture. (Fig. 6(a)). In this system, REASON serves as an efficient and reconfigurable “slow thinking” engine, accelerating symbolic and probabilistic kernels that are poorly suited to GPU execution. As illustrated in Fig. 6(b), REASON comprises an array of tree-based PE cores that act as the primary computation engines. A global controller and workload scheduler manage the workload mapping. A shared local memory serves as a unified scratchpad for all cores. Communication between cores and shared memory is handled by a high-bandwidth global interconnect.

Tree architecture. Each PE core is organized as a tree-structured compute engine, as shown in Fig. 6(c). Each tree node integrates a specialized datapath, memory subsystem, and control logic optimized for executing DAG-based symbolic and probabilistic operations.

Reconfigurable tree engine (RTE). At the core of each PE is a Reconfigurable Tree Engine (RTE), whose datapath forms a bidirectional tree of PEs (Fig. 6(d)). The RTE supports both SAT-style symbolic broadcast patterns and probabilistic aggregation operations. A Benes network interconnect enables N-to-N routing, decoupling SRAM banking from DAG mapping and simplifying compilation of irregular graph structures (Sec. V-C). Forwarding logic routes intermediate and irregular outputs back to SRAM for subsequent batches.

Memory subsystem. To tackle the memory-bound nature of symbolic and probabilistic kernels, the RTE is backed by a set of dual-port, wide-bitline SRAM banks arranged as a banked L1 cache. A memory front-end with a prefetcher and high-throughput DMA engine moves data from shared scratchpad. A control/memory management unit (MMU) block handles address translation across the distributed memory system.

Core control and execution. A scalar PE acts as the core-level controller, fetching and issuing VLIW-like instructions that configure the RTE, memory subsystem, and specialized units. Outputs from the RTE are buffered before being consumed by the scalar PE or the SIMD Unit, which provides support for executing parallelizable subset of symbolic solvers.

B. Reconfigurable Symbolic/Probabilistic PE

The PE architecture is designed to support a wide range of symbolic and probabilistic computation patterns via a VLIW-driven cycle-reconfigurable datapath. Each PE can switch

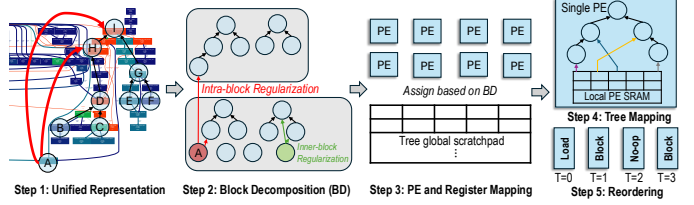


Fig. 7: Compiler-architecture co-design for probabilistic execution. A probabilistic DAG is decomposed, regularized, mapped onto tree-based PEs, and scheduled with pipeline awareness to enable efficient execution of irregular probabilistic kernels in REASON.

among three operational modes to efficiently execute heterogeneous kernels mapped from the unified DAG representation.

Probabilistic mode. In probabilistic mode, the node executes irregular DAGs derived from unified probabilistic representations (Sec. V-C). The nodes are programmed by the VLIW instruction stream to perform arithmetic operations, either addition or multiplication, required by the DAG node mapped onto them. This mode supports probabilistic aggregation patterns such as sum-product computation and likelihood propagation, enabling efficient execution of PCs and HMMs.

Symbolic mode. In symbolic mode, the datapath is repurposed for logical reasoning operations (Sec. V-D). Key hardware components are utilized as follows: (a) The comparator checks logical states for Boolean Constraint Propagation (BCP), identifying literals as TRUE, FALSE, or UNASSIGNED. (b) The adder performs two key functions: address computation by adding the Clause Base Address and Literal Index to locate the next literal in a clause; and clause evaluation by acting as counter to track the number of FALSE literals. This enables fast detection of unit clauses and conflicts, accelerating SAT-style symbolic reasoning.

SpMSpM mode. The tree-structured PE inherently supports the sparse matrix-matrix multiplication (SpMSpM), a computation pattern widely studied in prior works [39], [40]. In this mode, the leaf nodes are configured as multipliers to compute partial products of the input matrix elements, while the internal nodes are configured as adders to perform hierarchical reductions. This execution pattern allows small-scale neural or neural-symbolic models to be efficiently mapped onto the REASON engine, extending its applicability beyond purely symbolic and probabilistic kernels.

C. Architectural Support for Probabilistic Reasoning

Probabilistic reasoning kernels are expressed as DAGs composed of arithmetic nodes (sum and product) connected by data-dependent edges. REASON exploits its pipelined, tree-structured datapath to efficiently map these DAGs onto parallel PEs. Key architectural features include: multi-tree PE mapping for arithmetic DAG execution, a banked register file with flexible crossbar interconnect to support irregular memory access, and compiler-assisted pipeline scheduling with automatic register management to reduce control overhead. Fig. 7 illustrates the overall workflow.

Datapath and pipelined execution. The datapath operates in a pipelined fashion, with each layer of nodes serving as

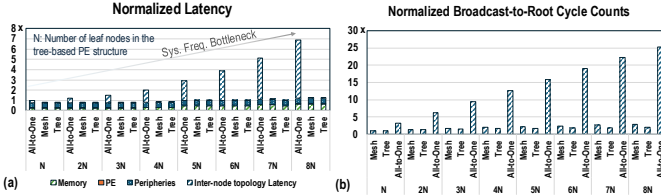


Fig. 8: Scalability analysis of interconnect topologies. (a) Normalized latency breakdown as the number of leaf nodes N increases. (b) Normalized broadcast-to-root cycle counts for different PE interconnect structures.

pipeline stages. Each pipeline stage receives inputs from a banked register file, which consists of multiple parallel register banks. Each bank operates independently, providing flexible addressing that accommodates the irregular memory access patterns typical in probabilistic workloads (e.g., PCs, HMMs).

Flexible interconnect. To handle the irregularity in probabilistic DAGs, REASON employs an optimized interconnection. An input Benes crossbar connects the register file banks to inputs of PE trees, allowing flexible and conflict-free routing of operands into computation units. Output connections from PE to register banks are structured as one-bank-one-PE to minimize hardware complexity while preserving flexibility, balancing trade-offs between utilization and performance.

Register management. REASON adopts an automatic write-address generation policy. Data is written to the lowest available register address in each bank, eliminating the need to encode explicit write addresses in instructions. The compiler precisely predicts these write addresses at compile time due to the deterministic execution sequence, further reducing instruction size and energy overhead.

Compiler-driven optimization. To efficiently translate unified DAGs into executable kernels and map onto hardware datapath, REASON adopts a four-step compiler pipeline (Fig. 7).

Step-1 Block decomposition: The compiler decomposes the unified DAG from Sec. IV into execution blocks through a greedy search that identifies schedulable subgraphs whose maximum depth does not exceed the hardware tree depth. This process maximizes PE utilization while minimizing inter-block dependencies that may cause read-after-write stalls. The resulting tree-like blocks form the basis for efficient mapping.

Step-2 PE mapping: For each block, the compiler jointly assigns nodes to PEs and operands to register banks, considering topological constraints and datapath connectivity. Nodes are mapped to preserve order, while operands are allocated to banks to avoid simultaneous conflicts. The compiler dynamically updates feasible mappings and prioritizes nodes with the fewest valid options. This conflict-aware strategy minimizes bank contention and balances data traffic across banks.

Step-3 Tree mapping: Once block and register mappings are fixed, the compiler constructs physical compute trees that maximize data reuse in the REASON datapath. Node fusion and selective replication enhance operand locality and reduce inter-block communication, allowing intermediate results to be consumed within the datapath and lowering memory traffic.

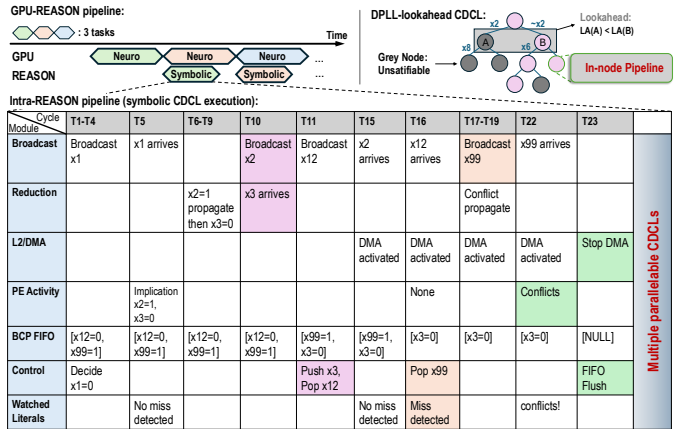


Fig. 9: Two-level execution pipeline for symbolic reasoning. Top: task-level overlap between GPU neural execution and REASON symbolic execution. Bottom: detailed cycle-by-cycle timeline of CDCL SAT solving, illustrating pipelined broadcast/reduction, WLs traversal, latency hiding, and priority-based conflict handling. Color represents the causality of hardware events.

Step-4 Reordering: The compiler then schedules instructions with awareness of the multi-stage pipeline. Dependent operations are spaced by at least one full pipeline interval, while independent ones are interleaved. Lightweight load, store, and copy operations fill idle cycles without disturbing dependencies. Live-range analysis identifies register pressure and inserts minimal spill and reload instructions when needed.

The DAG-to-hardware mapping is an automated heuristic process to generate a compact VLIW program for REASON. Designers can interact for design-space exploration to tune architectural parameters within flexible hardware template.

D. Architectural Support for Symbolic Logical Reasoning

To efficiently support symbolic logical reasoning kernels, REASON features a linked-list-based memory layout and hardware-managed BCP FIFO mechanism (Fig. 6(e)), enabling efficient and scalable support to large-scale solver kernels that are fundamental to logical reasoning.

Watched literals (WLs) unit. The WLs unit acts as a distributed memory controller tightly integrated with N SRAM banks, implementing the two-watched-literals indexing scheme in hardware. This design transforms the primary bottleneck in BCP from a sequential scan over the clause database into a selective parallel memory access problem. Crucially, it enables scalability to industrial-scale SAT problems [41], where only a small subset of clauses (those on the watch list) need to be accessed at any time. This design naturally aligns with a hierarchical memory system, allowing most clauses to reside in remote scratchpad memory or DRAM, with on-chip SRAM caching only the required clauses indexed by WLs unit.

SRAM layout. The local SRAM is partitioned to support a linked-list-based organization of watch lists. A dedicated region stores a head pointer table indexed by literal IDs, each pointing to the start of a watch list, enabling $\mathcal{O}(1)$ access. The main data region stores clauses, each augmented with a next-watch pointer that links to other clauses watching the same

Listing 1: C++ Programming Interface of REASON

```

// Trigger symbolic execution for a single inference
void REASON_execute(
    int batch_id, // batch identifier
    int batch_size, // number of objects in the batch
    const void* neural_buffer, // neural results in
        shared memory
    const void* reasoning_mode, // mode selection
    void* symbolic_buffer // write-back symb. results
);
// Query current REASON status for a given object
int REASON_check_status (
    int batch_id, // batch identifier
    bool blocking // wait till REASON is idle
);

```

literal, forming multiple linked lists within the linear address space. Upon a variable assignment, the WLs unit uses the literal ID to fetch the head pointer and traverses the list by following next-watch pointers, dispatching only the relevant clause to PEs. This hardware-managed indexing eliminates full-database scans and maps efficiently to the adder datapath.

BCP FIFO. The BCP FIFO sits atop the M:1 output interconnect (Fig. 6(c)) and serializes multiple parallel implications generated by the leaf tree-node in a single cycle. While many implications can be discovered concurrently, BCP must propagate them sequentially to preserve the causality chain for conflict analysis. The controller immediately broadcasts one implication back into the pipeline, while the rest are queued in the FIFO and processed in a pipelined manner. Within a symbolic (DPLL) tree node, implications are causally independent and can be pipelined, but between assignments, sequential ordering is enforced to maintain correctness. Sec. V-E illustrates a detailed cycle-level execution example.

Scalability advantages. A key advantage of the REASON architecture is that its tree-based inter-node topology does not become a bottleneck as the symbolic DPLL tree grows (Fig. 8(a)). In contrast, all-to-one (or one-to-all) bus interconnects often fail to scale due to post-layout electrical constraints, including high fan-out and buffer insertion for hold-time fixes. Moreover, given that broadcasting is a dominant operation, the root-to-leaf traversal latency is critical. REASON’s tree-based inter-node topology achieves exceptional scalability with an $\mathcal{O}(\log N)$ traversal latency, compared to $\mathcal{O}(\sqrt{N})$ for mesh-based designs and $\mathcal{O}(N)$ for bus-based interconnects (Fig. 8(b)). This property enables robust scalability for large symbolic reasoning workloads.

E. Case Study: A Working Example of Symbolic Execution

Fig. 9 illustrates the dynamic, pipelined per-node execution of REASON during a cube-and-conquer SAT solving phase, which highlights several key hardware mechanisms, including inter-node pipelined broadcast/reduction, latency hiding via parallel WLs traversal, and priority-based conflict handling.

Execution begins with the controller issuing a Decision to assign x_1 , which is broadcast through the distribution tree (T1–T4). At T5, leaf nodes concurrently discover two implications: $x_2=1$ and $x_3=0$. These implications are returned

to the controller via the reduction tree in a pipelined manner, where $x_2=1$ arrives first, followed by $x_3=0$ at T10. Since the FIFO is occupied, $x_3=0$ is queued into the BCP FIFO at T11.

At T15, the FIFO pops a subsequent implication (x_{12}), which triggers WLs lookup. A local SRAM miss prompts the L2/DMA to begin fetching clause, meanwhile BCP FIFO continues servicing queued implications: x_{99} is popped and broadcast from T17–T19 while DMA fetch is still in progress.

At T22, the propagation of x_{99} results in a Conflict, which immediately propagates up the reduction tree. Upon receiving the conflict signal at T23, the controller asserts priority control: it halts the ongoing DMA fetch, flushes the FIFO, and discards all pending implications (including $x_3=0$) from the now-invalid search path. The cube-and-conquer phase terminates, and the parallelized DPLL node is forwarded to the scalar PE for CDCL conflict analysis, as discussed in Sec. II-C.

F. Design Space Exploration and Scalability

Design space exploration. To identify the optimal configuration of REASON architecture, we perform a comprehensive design space exploration. We systematically evaluated different configurations by varying key architectural parameters such as the depth of the tree (D), the number of parallel register banks (B), and the number of registers per bank (R). We evaluate each configuration across latency, energy consumption, and energy-delay product (EDP) on representative workloads. The selected configuration (D=3, B=64, R=32) offers the optimal trade-off between performance and energy efficiency.

Scalability and variability support. Coupled with reconfigurable array, pipeling scheduling, and memory layout optimizations, REASON provides flexible hardware support across symbolic and probabilistic kernels (e.g., SAT, FOL, PC, HMM), neuro-symbolic workloads, and cognitive tasks, enabling efficient neuro-symbolic processing at scale (Sec. VII).

Design choice discussion. We adopt a unified architecture for symbolic and probabilistic reasoning to maximize flexibility and efficiency, rather than decoupling them into separate engines. We identify these kernels share common DAG patterns, enabling REASON to execute them on Tree-PEs through a unified representation. This approach achieves >90% utilization with 58% lower area/power than decoupled designs, while maintaining tight symbolic-probabilistic coupling. A flexible Benes network and compiler co-design handle routing and memory scheduling, ensuring efficient execution.

VI. REASON: SYSTEM INTEGRATION AND PIPELINE

This section presents the system-level integration of REASON. We first present the integration principles and workload partitioning strategy between GPU and REASON (Sec. VI-A), then introduce the programming model that enables flexible invocation and synchronization (Sec. VI-B). Finally, we describe the two-level execution pipeline (Sec. VI-C).

A. Integration with GPUs for End-to-End Reasoning

Integration principles. As illustrated in Fig. 6(a), the proposed REASON is integrated as a co-processor within

GPU system to support efficient end-to-end symbolic and probabilistic reasoning. This integration follows two principles: (1) *Versatility* to ensure compatibility with a broad range of logical and probabilistic reasoning workloads in neuro-symbolic pipelines, and (2) *Efficiency* to achieve low-latency execution for real-time reasoning. These principles necessitate careful workload assignment between GPU and REASON with pipelined execution.

Workload partitioning. To maximize performance while preserving compatibility with existing and emerging LLM-based neuro-symbolic agentic pipelines, we assign neural computation (e.g., LLM inference) to the GPU and offload symbolic reasoning and probabilistic inference to REASON. This partitioning exploits the GPU’s high throughput and programmability for neural kernels, while leveraging REASON’s reconfigurable architecture optimized for logical and probabilistic operations. It also minimizes data movement and enables pipelined execution: while REASON processes symbolic reasoning for the current batch, the GPU concurrently executes neural computation for the next batch.

B. Programming Model

REASON’s programming model (Listing. 1) is designed to offer full flexibility and control, making it easy to utilize REASON for accelerating various neuro-symbolic applications. It exposes two core functions for executing and status checking, enabling acceleration of logical and probabilistic kernels.

REASON_execute is responsible for processing a single symbolic reasoning run. It is called after GPU SMs complete processing the neural LLM. REASON then performs logical reasoning and probabilistic inference, and writes the symbolic results to shared memory, where SMs use for the next iteration.

REASON_check_status reports the current execution status of REASON (IDLE or EXECUTION) and includes an optional blocking flag. This feature allows the host thread to wait for REASON to complete the current step of reasoning before starting the next, ensuring proper coordination across subtasks without relying on CUDA stream synchronization.

Synchronization. Coordination between SMs and REASON is handled through shared-memory flag buffers and L2 cache. After executing LLM kernel, SMs write the output to shared memory and set `neural_ready` flag. REASON polls this flag, fetches the data, and performs symbolic reasoning. It then writes the result back to shared memory and sets `symbolic_ready` flag, which will be retrieved for final output. This tightly coupled design leverages GPU’s throughput for LLM kernels and REASON’s efficiency for symbolic reasoning, minimizing overhead and maximizing performance.

C. Two-Level Execution Pipeline

Our system-level design employs a two-level pipelined execution model (Fig. 9 top-left) to maximize concurrency across neural and symbolic kernels. The *GPU-REASON pipeline* overlaps the execution of symbolic kernels on REASON for step N with neural kernels on GPU for step $N+1$, effectively hiding the latency of one stage and improving throughput.

TABLE III: Hardware baselines. Comparison of device specs.

Device	Technology	SRAM	Number of Cores	Area [mm ²]	Power [W]
Orin NX [42]	8 nm	4 MB	512 CUDA Cores	450	15
RTX A6000 [43]	8 nm	16.5 MB	10572 CUDA Cores	628	300
Xeon CPU [44]	10 nm	112.5 MB	60 cores per socket	1600	270
TPU [45]	7 nm	170 MB	8 128×128 PEs	400	192
DPU [#] [46]	28 nm	2.4 MB	8 PEs / 56 Nodes	3.20	1.10
REASON	28 nm	1.25 MB	12 PEs / 80 Nodes	6.00	2.12
REASON [*]	12 nm	1.25 MB	12 PEs / 80 Nodes	1.37	1.21
REASON [*]	8 nm	1.25 MB	12 PEs / 80 Nodes	0.51	0.98

^{*} The 12nm and 8nm data are scaled from the *DeepScaleTool* [47] with a voltage of 0.8V and a frequency of 500MHz. [#] The terminology for tree-based architecture is renamed from tree to PE and PE to node to align with the proposed REASON.

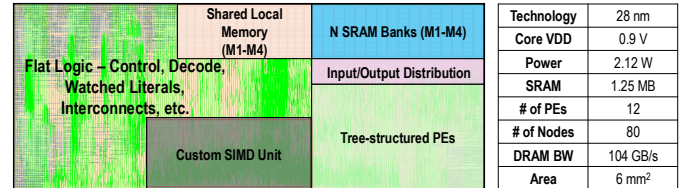


Fig. 10: REASON layout and specifications. The physical design and key operating specifications of our proposed REASON hardware.

Within REASON, the *Intra-REASON pipeline* exploits inter-node pipelined broadcast and reduction to hide communication latency, using parallel worklist traversal and priority-based conflict handling to accelerate symbolic kernels (Sec. V-E). The compiler integrates pipeline-aware scheduling to reorder instructions, avoid read-after-write hazards, and insert no-operation instructions when necessary, ensuring each stage receives valid data without interruption.

VII. EVALUATION

This section introduces REASON evaluation settings (Sec. VII-A), and benchmarks the proposed algorithm optimizations (Sec. VII-B) and hardware architecture (Sec. VII-C).

A. Evaluation Setup

Datasets. We evaluate REASON on 10 commonly-used reasoning datasets: IMO [15], MiniF2F [48], TwinSafety [22], XSTest [49], CommonGen [50], News [51], CoAuthor [52], AwA2 [53], FOLIO [54], and ProofWriter [55]. The tasks are measured by the reasoning and deductive accuracy.

Algorithm setup. We evaluate REASON on six state-of-the-art neuro-symbolic models, i.e., AlphaGeometry [15], R²-Guard [22], GeLaTo [29], Ctrl-G [23], NeuroPC [30], and LINC [31]. Following the setup in the original literature, we determine the hyperparameters based on end-to-end reasoning performance on the datasets. Our proposed REASON algorithm optimizations are general and can work as a plug-and-play extension to existing neuro-symbolic algorithms.

Baselines. We consider several hardware baselines, including Orin NX [42] (since our goal is to enable real-time neuro-symbolic at edge), RTX GPU [43], Xeon CPU [44], ML accelerators (TPU [45], DPU [46]). Tab. III lists configurations.

Hardware setup. We implement REASON architecture with [46] as the baseline template, synthesize with Synopsys DC [56], and place and route using Cadence Innovus [57] at TSMC 28nm node. Fig. 10 illustrates the layout and key specifications. The REASON hardware consumes an area of 6 mm² and an average power of 2.12 W across workloads based

TABLE IV: REASON algorithm optimization performance. REASON achieves comparable accuracy with reduced memory footprint via unified DAG representation, adaptive pruning, and regularization.

Workloads	Benchmarks	Metrics	Baseline Performance	After REASON Algo. Opt.	Memory ↓
AlphaGeo	IMO	Accuracy (\uparrow)	83%	83%	25%
	MiniF2F	Accuracy (\uparrow)	81%	81%	21%
R ² -Guard	TwinSafety	AUPRC (\uparrow)	0.758	0.752	37%
	XTest	AUPRC (\uparrow)	0.878	0.881	30%
GeLaTo	CommonGen	BLEU (\uparrow)	30.3	30.2	41%
	News	BLEU (\uparrow)	5.4	5.4	27%
Ctrl-G	CoAuthor	Success rate (\uparrow)	87%	86%	29%
NeuroSP	AwA2	Accuracy	87%	87%	43%
LINC	FOLIO	Accuracy (\uparrow)	92%	91%	38%
	ProofWriter	Accuracy (\uparrow)	84%	84%	26%

on Synopsys PTPX [58] power-trace analysis (Fig. 12(a)). Unlike conventional tree-based arrays that mainly target neural workloads, REASON provides unified, reconfigurable support for neural, symbolic, and probabilistic computation.

Simulation setup. To evaluate end-to-end performance of REASON when integrated with GPUs, we develop a cycle-accurate simulator based on Accel-Sim (built on GPGPU-Sim) [59]. The simulator is configured for Orin NX architecture. The on-chip GPU is modeled with 8 SMs, each supporting 32 threads per warp, 48 KB shared memory, and 128 KB L1 cache, with a unified 2 MB L2 cache shared across SMs. The off-chip memory uses a 128-bit LPDDR5 interface with 104 GB/s peak BW. DRAM latency and energy are modeled using LPDDR5 timing parameters.

Simulator test trace derivation. We use GPGPU-Sim to model interactions between SMs and REASON, including transferring neural results from SMs to REASON and returning symbolic reasoning results from REASON to SMs. To simulate communication overhead, we extract memory access traces from neuro-symbolic model execution on Orin, capturing data volume and access patterns as inputs to GPGPU-Sim for accurate modeling. For GPU comparison baselines, we use real hardware measurements to get accurate ground-truth data.

B. REASON Algorithm Performance

Reasoning accuracy. To evaluate REASON algorithm optimization (Sec. IV), we benchmark it on ten reasoning tasks (Sec. VII-A). Tab. IV lists the arithmetic performance and DAG size reduction. We observe that REASON achieves comparable reasoning accuracy through unification and adaptive DAG pruning. Through pruning and regularization, REASON enables 31.7% memory footprint savings on average of ten reasoning tasks across six neuro-symbolic workloads.

C. REASON Architecture Performance

Performance improvement. We benchmark REASON accelerator with Orin NX, RTX GPU, and Xeon CPU for accelerating neuro-symbolic algorithms on 10 reasoning tasks (Fig. 11). For GPU baseline, for neuro kernels, we use Pytorch package that leverages CUDA and cuBLAS/cuDNN libraries; for symbolic kernels, we implement custom kernels optimized for logic and probabilistic operations. The workload is tiled by CuDNN in Pytorch based on block sizes that fit well in GPU memory. We observe that REASON exhibits consistent

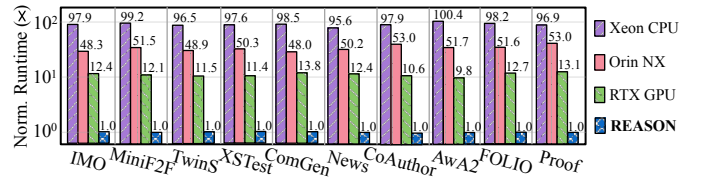


Fig. 11: End-to-end runtime improvement. REASON consistently outperforms Xeon CPU, Orin NX, and RTX GPU in end-to-end runtime latency evaluated on 10 logical and cognitive reasoning tasks.

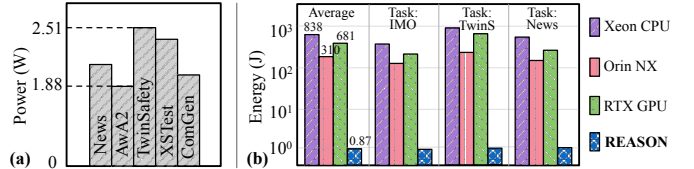


Fig. 12: Energy efficiency improvement. (a) Power analysis of REASON across workloads. (b) Energy efficiency comparison between REASON and CPUs/GPUs, evaluated from 10 reasoning tasks.

speedup across datasets, e.g., $50.65 \times / 11.98 \times$ speedup over Orin NX and RTX GPU. Furthermore, REASON achieves real-time performance (<1.0 s) on solving math and cognitive reasoning tasks, indicating that REASON enables real-time probabilistic logical reasoning-based neuro-symbolic system with superior reasoning and generalization capability, offering a promising solution for future cognitive applications.

Energy efficiency improvement. REASON accelerator achieves two orders of energy efficiency than Orin NX, RTX GPU, and Xeon CPU consistently across workloads (Fig. 12(b)). To further assess REASON energy efficiency in long-term deployment, we perform consecutive tests on REASON using mixed workloads, incorporating both low-activity and high-demand periods, with 15s idle intervals between scenarios. On average, REASON achieves $681 \times$ energy efficiency compared to RTX GPU. Additionally, when compared to V100 and A100, REASON shows $4.91 \times$ and $1.60 \times$ speedup, with $802 \times$ and $268 \times$ energy efficiency, respectively.

Compare with CPU+GPU. We compare the performance of REASON as GPU plug-in over the CPU+GPU architecture across neuro-symbolic workloads. CPU+GPU architecture is not efficient for neuro-symbolic computing due to (1) high latency of symbolic/probabilistic operations with poor locality and $<5\%$ CPU parallel efficiency, (2) $>15\%$ inter-device communication overhead from frequent neural-symbolic data transfers, and (3) fine-grained coupling between neural and symbolic modules that makes handoffs costly. REASON co-locates logical and probabilistic reasoning beside GPU SMs, sharing L2 and inter-SM fabric to eliminate transfers and pipeline neural-symbolic execution.

Compare with ML accelerators. We benchmark the runtime of neural and symbolic operations on TPU-like systolic array [45] and DPU-like tree-based array [46] over different neuro-symbolic models and tasks (Fig. 13). For TPU-like architecture, we use SCALE-Sim [60], configured with eight 128×128 systolic arrays. For DPU-like architecture, we use MAERI [39], configured with eight PEs in 56-node tree-based

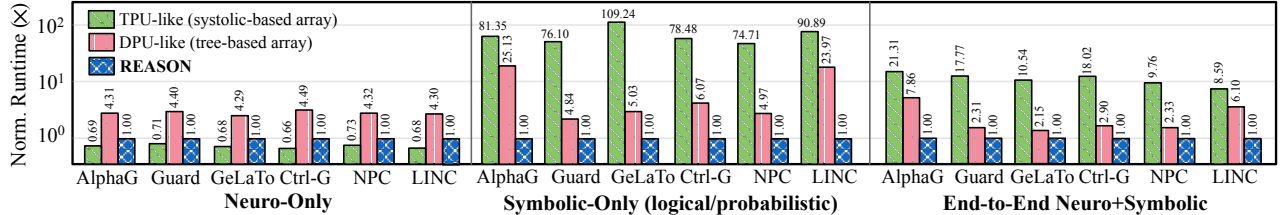


Fig. 13: Improved efficiency over ML accelerators. Speedup comparison of neural, symbolic (logical and probabilistic), and end-to-end neuro-symbolic system over TPU-like systolic-based array and DPU-like tree-based array architecture.

TABLE V: Ablation study of necessity of co-design. The normalized runtime achieved by REASON framework w/o the proposed algorithm optimization or hardware techniques on different tasks.

Neuro-symbolic System	Normalized Runtime (%) on				
Algorithm @ Hardware	IMO [15]	MiniF [48]	TwinS [22]	XSTest [49]	ComG [50]
[15], [22], [29] @ Orin NX	100	100	100	100	100
REASON Algo. @ Orin NX	84.2%	87.0%	78.3%	82.9%	86.6%
REASON Algo. @ REASON HW	2.07%	1.94%	2.04%	1.99%	2.08%

array. Compared with ML accelerators, we observe that REASON achieves similar performance in neural operations, while exhibiting superior symbolic logic and probabilistic operation efficiency thus end-to-end speedup in neuro-symbolic systems.

Ablation study on the proposed hardware techniques. REASON features reconfigurable tree-based array architecture, efficient register bank mapping, and adaptive scheduling strategy to reduce compute latency for neural, symbolic, and probabilistic kernels (Sec. V and Sec. VI). To demonstrate the effectiveness, we measure the runtime of REASON w/o the scheduling, reconfigurable architecture, and bank mapping. In particular, the proposed memory layout support can trim down the runtime by 22% on average. Additionally, with the proposed reconfigurable array and scheduling strategy, the runtime reduction ratio can be further enlarged to 56% and 73%, indicating that both techniques are necessary for REASON to achieve the desired efficient reasoning capability.

Ablation study of the necessity of co-design. To verify the necessity of algorithm-hardware co-design strategy to achieve efficient probabilistic logical reasoning-based neuro-symbolic systems, we measure the runtime latency of our REASON w/o the proposed algorithm or hardware techniques in Tab. V. Specifically, with our proposed REASON algorithm optimization, we can trim down the runtime to 78.3% as compared to R²-Guard [22] on the same Orin NX hardware and TwinSafety task. Moreover, with both proposed REASON algorithm optimization and accelerator, the runtime can be reduced to 2.04%, indicating the necessity of the co-design strategy of REASON framework.

REASON neural optimization. REASON accelerates symbolic reasoning and enables seamless interaction with GPU optimized for neuro (NN/LLM) computation. To further optimize neural module, we integrate standard LLM acceleration techniques: memory-efficient attention [61], chunked prefill [62], speculative decoding [63], FlashAttention-3 kernels [64], FP8 KV-Cache quantization [65], and prefix caching [66]. These collectively yield 2.8-3.3 \times latency reduction for unique prompts and 4-5 \times when prefixes are reused. While REASON’s reported gains stem from its hardware-software co-design,

these LLM optimizations are orthogonal and can be applied in conjunction to unlock full potential system speedup.

VIII. RELATED WORK

Neuro-symbolic AI. Neuro-symbolic AI has emerged as a promising paradigm for addressing limitations of purely neural models, including factual errors, limited interpretability, and weak multi-step reasoning. [67]–[73]. Systems such as LIPS [14], AlphaGeometry [15], NSC [74], NS3D [75] demonstrate strong performance across domains ranging from mathematical reasoning to embodied and cognitive robotics. However, most prior work focuses on algorithmic design and model integration. *REASON systematically characterizing the architectural and system-level properties of probabilistic logical reasoning in neuro-symbolic AI, and proposes an integrated acceleration framework for scalable deployment.*

System and architecture for neuro-symbolic AI. Early neuro-symbolic systems largely focused on software-level abstractions, such as training semantics and declarative languages that integrate neural with logical or probabilistic reasoning, such as DeepProbLog [76], DreamCoder [77], and Scallop [78]. Recent efforts have begun to address system-level challenges, such as heterogeneous mapping, batching control-heavy reasoning, and kernel specialization, including benchmarking [79], pruning [80], Lobster [81], Dolphin [82], and Klay [83]. At the architectural level, a growing body of work exposes the mismatch between compositional neuro-symbolic workloads and conventional hardware designs, motivating cognitive architectures such as CogSys [84], NVSA architectures [85], and NSFlow [86]. *REASON advances this direction with the first flexible system-architecture co-design that supports probabilistic logical reasoning-based neuro-symbolic AI and integrates with GPU, enabling efficient and scalable compositional neuro-symbolic and LLM+tools agentic system deployment.*

IX. CONCLUSION

We present REASON, the integrated acceleration framework for efficiently executing probabilistic logical reasoning in neuro-symbolic AI. REASON introduces a unified DAG abstraction with adaptive pruning and a flexible reconfigurable architecture integrated with GPUs to enable efficient end-to-end execution. Results show that system-architecture co-design is critical for making neuro-symbolic reasoning practical at scale, and position REASON as a potential foundation for future agentic AI and LLM+tools systems that require structured and interpretable reasoning alongside neural computation.

ACKNOWLEDGEMENTS

This work was supported in part by CoCoSys, one of seven centers in JUMP 2.0, a Semiconductor Research Corporation (SRC) program sponsored by DARPA. We thank Ananda Samajdar, Ritik Raj, Anand Raghunathan, Kaushik Roy, Ningyuan Cao, Katie Zhao, Alexey Tumanov, Shirui Zhao, Xiaoxuan Yang, Zhe Zeng, and the anonymous HPCA reviewers for insightful discussions and valuable feedback.

REFERENCES

- [1] Jiayi Kuang, Ying Shen, Jingyou Xie, Haohao Luo, Zhe Xu, Ronghao Li, Yinghui Li, Xianfeng Cheng, Xika Lin, and Yu Han. Natural language understanding and inference with milm in visual question answering: A survey. *ACM Computing Surveys*, 57(8):1–36, 2025.
- [2] Muhammad Ferjad Naeem, Muhammad Gul Zain Ali Khan, Yongqin Xian, Muhammad Zeshan Afzal, Didier Stricker, Luc Van Gool, and Federico Tombari. I2mvformer: Large language model generated multi-view document supervision for zero-shot image classification. In *Proceedings of the IEEE/CVF Conference on Computer Vision and Pattern Recognition*, pages 15169–15179, 2023.
- [3] Suvir Mirchandani, Fei Xia, Pete Florence, Brian Ichter, Danny Driess, Montserrat Gonzalez Arenas, Kanishka Rao, Dorsa Sadigh, and Andy Zeng. Large language models as general pattern machines. *CoRL*, 2023.
- [4] Mohamed Ibrahim, Zishen Wan, Haitong Li, Priyadarshini Panda, Tushar Krishna, Penti Kanerva, Yiran Chen, and Arijit Raychowdhury. Special session: Neuro-symbolic architecture meets large language models: A memory-centric perspective. In *2024 International Conference on Hardware/Software Codesign and System Synthesis (CODES+ ISSS)*, pages 11–20. IEEE, 2024.
- [5] Matéo Mahaut, Laura Aina, Paula Czarnowska, Momchil Hardalov, Thomas Müller, and Lluís Márquez. Factual confidence of llms: on reliability and robustness of current estimators. *ACL*, 2024.
- [6] Gaurang Sriramanan, Siddhant Bharti, Vinu Sankar Sadasivan, Shoumik Saha, Priyatham Kattakinda, and Soheil Feizi. Llm-check: Investigating detection of hallucinations in large language models. *Advances in Neural Information Processing Systems*, 37:34188–34216, 2024.
- [7] Renat Aksitov, Sobhan Miryoosfi, Zonglin Li, Daliang Li, Sheila Babayan, Kavya Kopparapu, Zachary Fisher, Ruiqi Guo, Sushant Prakash, Pranesh Srinivasan, et al. Rest meets react: Self-improvement for multi-step reasoning llm agent. *arXiv preprint arXiv:2312.10003*, 2023.
- [8] Chandan Singh, Jeevana Priya Inala, Michel Galley, Rich Caruana, and Jianfeng Gao. Rethinking interpretability in the era of large language models. *arXiv preprint arXiv:2402.01761*, 2024.
- [9] Chen Shengyuan, Yunfeng Cai, Huang Fang, Xiao Huang, and Mingming Sun. Differentiable neuro-symbolic reasoning on large-scale knowledge graphs. *Advances in Neural Information Processing Systems*, 36:28139–28154, 2023.
- [10] Kareem Ahmed, Stefano Teso, Kai-Wei Chang, Guy Van den Broeck, and Antonio Vergari. Semantic probabilistic layers for neuro-symbolic learning. *Advances in Neural Information Processing Systems*, 35:29944–29959, 2022.
- [11] Zishen Wan, Che-Kai Liu, Hanchen Yang, Chaojian Li, Haoran You, Yonggan Fu, Cheng Wan, Tushar Krishna, Yingyan Lin, and Arijit Raychowdhury. Towards cognitive ai systems: a survey and prospective on neuro-symbolic ai. *arXiv preprint arXiv:2401.01040*, 2024.
- [12] Shuting Du, Mohamed Ibrahim, Zishen Wan, Luqi Zheng, Boheng Zhao, Zhenkun Fan, Che-Kai Liu, Tushar Krishna, Arijit Raychowdhury, and Haitong Li. Cross-layer design of vector-symbolic computing: Bridging cognition and brain-inspired hardware acceleration. *arXiv preprint arXiv:2508.14245*, 2025.
- [13] Zishen Wan, Che-Kai Liu, Hanchen Yang, Ritik Raj, Arijit Raychowdhury, and Tushar Krishna. Efficient processing of neuro-symbolic ai: A tutorial and cross-layer co-design case study. *Proceedings of the International Conference on Neuro-symbolic Systems*, 2025.
- [14] Zenan Li, Zhaoyu Li, Wen Tang, Xian Zhang, Yuan Yao, Xujie Si, Fan Yang, Kaiyu Yang, and Xiaoxing Ma. Proving olympiad inequalities by synergizing llms and symbolic reasoning. *International Conference on Learning Representations (ICLR)*, pages 1–26, 2025.
- [15] Trieu H Trinh, Yuhuai Wu, Quoc V Le, He He, and Thang Luong. Solving olympiad geometry without human demonstrations. *Nature*, 625(7995):476–482, 2024.
- [16] Bernardino Romera-Paredes, Mohammadamin Barekatain, Alexander Novikov, Matej Balog, M Pawan Kumar, Emilien Dupont, Francisco JR Ruiz, Jordan S Ellenberg, Pengming Wang, Omar Fawzi, et al. Mathematical discoveries from program search with large language models. *Nature*, 625(7995):468–475, 2024.
- [17] Chi Zhang, Baoxiong Jia, Song-Chun Zhu, and Yixin Zhu. Abstract spatial-temporal reasoning via probabilistic abduction and execution. In *Proceedings of the IEEE/CVF Conference on Computer Vision and Pattern Recognition (CVPR)*, pages 9736–9746, 2021.
- [18] Michael Hersche, Mustafa Zeqiri, Luca Benini, Abu Sebastian, and Abbas Rahimi. A neuro-vector-symbolic architecture for solving raven’s progressive matrices. *Nature Machine Intelligence*, 5(4):363–375, 2023.
- [19] Jiayuan Mao, Chuang Gan, Pushmeet Kohli, Joshua B Tenenbaum, and Jiajun Wu. The neuro-symbolic concept learner: Interpreting scenes, words, and sentences from natural supervision. *International Conference on Learning Representations (ICLR)*, 2019.
- [20] Lingjie Mei, Jiayuan Mao, Ziqi Wang, Chuang Gan, and Joshua B Tenenbaum. Falcon: fast visual concept learning by integrating images, linguistic descriptions, and conceptual relations. *International Conference on Learning Representations (ICLR)*, 2022.
- [21] Zishen Wan, Yuhang Du, Mohamed Ibrahim, Jiayi Qian, Jason Jabbour, Yang Zhao, Tushar Krishna, Arijit Raychowdhury, and Vijay Janapa Reddi. Reca: Integrated acceleration for real-time and efficient cooperative embodied autonomous agents. In *Proceedings of the 30th ACM International Conference on Architectural Support for Programming Languages and Operating Systems (ASPLOS)*, Volume 2, pages 982–997, 2025.
- [22] Mintong Kang and Bo Li. R²-guard: Robust reasoning enabled llm guardrail via knowledge-enhanced logical reasoning. *International Conference on Learning Representations (ICLR)*, 2025.
- [23] Honghua Zhang, Po-Nien Kung, Masahiro Yoshida, Guy Van den Broeck, and Nanyun Peng. Adaptable logical control for large language models. *Advances in Neural Information Processing Systems (NeurIPS)*, 37:115563–115587, 2024.
- [24] Zishen Wan, Hanchen Yang, Jiayi Qian, Ritik Raj, Joongun Park, Chenyu Wang, Arijit Raychowdhury, and Tushar Krishna. Compositional ai beyond llms: System implications of neuro-symbolic-probabilistic architectures. In *Proceedings of the 31st ACM International Conference on Architectural Support for Programming Languages and Operating Systems (ASPLOS)*, Volume 1, pages 67–84, 2026.
- [25] Joao Marques-Silva, Inês Lynce, and Sharad Malik. Conflict-driven clause learning sat solvers. In *Handbook of satisfiability*, pages 133–182. Ios Press, 2021.
- [26] Michael Lo, Mau-Chung Frank Chang, and Jason Cong. Sat-accel: A modern sat solver on a fpga. In *Proceedings of the 2025 ACM/SIGDA International Symposium on Field Programmable Gate Arrays*, pages 234–246, 2025.
- [27] Marijn JH Heule, Oliver Kullmann, Siert Wieringa, and Armin Biere. Cube and conquer: Guiding cdcl sat solvers by lookaheads. In *Haifa Verification Conference*, pages 50–65. Springer, 2011.
- [28] Peter Van Der Tak, Marijn JH Heule, and Armin Biere. Concurrent cube-and-conquer. In *International Conference on Theory and Applications of Satisfiability Testing*, pages 475–476. Springer, 2012.
- [29] Honghua Zhang, Meihua Dang, Nanyun Peng, and Guy Van den Broeck. Tractable control for autoregressive language generation. In *International Conference on Machine Learning (ICML)*, pages 40932–40945. PMLR, 2023.
- [30] Weixin Chen, Simon Yu, Huajie Shao, Lui Sha, and Han Zhao. Neural probabilistic circuits: Enabling compositional and interpretable predictions through logical reasoning. *arXiv preprint arXiv:2501.07021*, 2025.
- [31] Theo X Olaussen, Alex Gu, Benjamin Lipkin, Cedegao E Zhang, Armando Solar-Lezama, Joshua B Tenenbaum, and Roger Levy. Linc: A neurosymbolic approach for logical reasoning by combining language models with first-order logic provers. *Conference on Empirical Methods in Natural Language Processing (EMNLP)*, 2023.
- [32] Yitao Liang and Guy Van den Broeck. Learning logistic circuits. In *Proceedings of the AAAI Conference on Artificial Intelligence*, volume 33, pages 4277–4286, 2019.
- [33] Pasha Khosravi, YooJung Choi, Yitao Liang, Antonio Vergari, and Guy Van den Broeck. On tractable computation of expected predictions. *Advances in Neural Information Processing Systems*, 32, 2019.

[34] Anji Liu, Kareem Ahmed, and Guy Van den Broeck. Scaling tractable probabilistic circuits: A systems perspective. *International Conference on Machine Learning (ICML)*, pages 30630–30646, 2024.

[35] Bhavya Mor, Sunita Garhwal, and Ajay Kumar. A systematic review of hidden markov models and their applications. *Archives of computational methods in engineering*, 28(3):1429–1448, 2021.

[36] NVIDIA. NVIDIA Jetson Orin. <https://www.nvidia.com/en-us/autonomous-machines/embedded-systems/jetson-orin/>.

[37] NVIDIA. NVIDIA Nsight Systems. <https://developer.nvidia.com/nsight-systems>.

[38] NVIDIA. NVIDIA Nsight Compute. <https://developer.nvidia.com/nsight-compute>.

[39] Hyoukjun Kwon, Ananda Samajdar, and Tushar Krishna. Maeri: Enabling flexible dataflow mapping over dnn accelerators via reconfigurable interconnects. *ACM Sigplan Notices*, 53(2):461–475, 2018.

[40] Francisco Muñoz-Martínez, Raveesh Garg, Michael Pellauer, José L Abellán, Manuel E Acacio, and Tushar Krishna. Flexagon: A multi-dataflow sparse-sparse matrix multiplication accelerator for efficient dnn processing. In *Proceedings of the 28th ACM International Conference on Architectural Support for Programming Languages and Operating Systems, Volume 3*, pages 252–265, 2023.

[41] Matthew W Moskewicz, Conor F Madigan, Ying Zhao, Lintao Zhang, and Sharad Malik. Chaff: Engineering an efficient sat solver. In *Proceedings of the 38th annual Design Automation Conference*, pages 530–535, 2001.

[42] Jetson orin for next-gen robotics — nvidia. <https://www.nvidia.com/en-us/autonomous-machines/embedded-systems/jetson-orin/>. (Accessed on 04/02/2024).

[43] NVIDIA Corporation. Nvidia rtx a6000 graphics card. <https://www.nvidia.com/en-us/products/workstations/rtx-a6000/>, 2020.

[44] INTEL Corporation. 4th gen intel xeon scalable processors. <https://www.intel.com/content/www/us/en/ark/products/series/228622/4th-gen-intel-xeon-scalable-processors.html>, 2023.

[45] Norman P Jouppi, Doe Hyun Yoon, Matthew Ashcraft, Mark Gottschos, Thomas B Jablin, George Kurian, James Laudon, Sheng Li, Peter Ma, Xiaoyu Ma, et al. Ten lessons from three generations shaped google’s tpuv4i: Industrial product. In *2021 ACM/IEEE 48th Annual International Symposium on Computer Architecture (ISCA)*, pages 1–14. IEEE, 2021.

[46] Nimish Shah, Wannes Meert, and Marian Verhelst. Dpu-v2: Energy-efficient execution of irregular directed acyclic graphs. In *2023 55th IEEE/ACM International Symposium on Microarchitecture (MICRO)*, pages 1288–1307. IEEE, 2023.

[47] Satyabrata Sarangi and Bevan Baas. Deepscaletool: A tool for the accurate estimation of technology scaling in the deep-submicron era. In *2021 IEEE International Symposium on Circuits and Systems (ISCAS)*, pages 1–5. IEEE, 2021.

[48] Kunhao Zheng, Jesse Michael Han, and Stanislas Polu. Minif2f: a cross-system benchmark for formal olympiad-level mathematics. *arXiv preprint arXiv:2109.00110*, 2021.

[49] Paul Röttger, Hannah Rose Kirk, Bertie Vidgen, Giuseppe Attanasio, Federico Bianchi, and Dirk Hovy. Xtest: A test suite for identifying exaggerated safety behaviours in large language models. *arXiv preprint arXiv:2308.01263*, 2023.

[50] Bill Yuchen Lin, Wangchunshu Zhou, Ming Shen, Pei Zhou, Chandra Bhagavatula, Yejin Choi, and Xiang Ren. Commongen: A constrained text generation challenge for generative commonsense reasoning. *Findings of the Association for Computational Linguistics (EMNLP)*, pages 1823—1840, 2020.

[51] Yizhe Zhang, Guoyin Wang, Chunyuan Li, Zhe Gan, Chris Brockett, and Bill Dolan. Pointer: Constrained progressive text generation via insertion-based generative pre-training. *arXiv preprint arXiv:2005.00558*, 2020.

[52] Mina Lee, Percy Liang, and Qian Yang. Coauthor: Designing a human-ai collaborative writing dataset for exploring language model capabilities. In *Proceedings of the 2022 CHI conference on human factors in computing systems*, pages 1–19, 2022.

[53] Y Xian, CH Lampert, B Schiele, and Z Akata. Zero-shotlearning—a comprehensive evaluation of the good, the bad and the ugly. *arXiv preprint arXiv:1707.00600*, 2018.

[54] Simeng Han, Hailey Schoelkopf, Yilun Zhao, Zhenting Qi, Martin Riddell, Wenfei Zhou, James Coady, David Peng, Yujie Qiao, Luke Benson, et al. Folio: Natural language reasoning with first-order logic. *arXiv preprint arXiv:2209.00840*, 2022.

[55] Oyvind Tafjord, Bhavana Dalvi Mishra, and Peter Clark. Proofwriter: Generating implications, proofs, and abductive statements over natural language. *arXiv preprint arXiv:2012.13048*, 2020.

[56] Synopsys. Design compiler - synopsys. <https://www.synopsys.com/implementation-and-signoff/rtl-synthesis-test/dc-ultra.html>.

[57] Cadence. Innovus implementation system - cadence. https://www.cadence.com/en_US/home/tools/digital-design-and-signoff/soc-implementation-and-floorplanning/innovus-implementation-system.html.

[58] Synopsys. Primetime - synopsys. <https://www.synopsys.com/implementation-and-signoff/signoff/primetime.html>.

[59] Mahmoud Khairy, Zhesheng Shen, Tor M Aamodt, and Timothy G Rogers. Accel-sim: An extensible simulation framework for validated gpu modeling. In *2020 ACM/IEEE 47th Annual International Symposium on Computer Architecture (ISCA)*, pages 473–486. IEEE, 2020.

[60] Ritik Raj, Sarbartha Banerjee, Nikhil Chandra, Zishen Wan, Jianming Tong, Ananda Samajdar, and Tushar Krishna. Scale-sim v3: A modular cycle-accurate systolic accelerator simulator for end-to-end system analysis. In *2025 IEEE International Symposium on Performance Analysis of Systems and Software (ISPASS)*, pages 186–200. IEEE, 2025.

[61] Woosuk Kwon, Zhuohan Li, Siyuan Zhuang, Ying Sheng, Lianmin Zheng, Cody Hao Yu, Joseph Gonzalez, Hao Zhang, and Ion Stoica. Efficient memory management for large language model serving with pagedattention. In *Proceedings of the 29th symposium on operating systems principles (SOSP)*, pages 611–626, 2023.

[62] vLLM. vLLM Performance and Tuning . <https://docs.vllm.ai/en/latest/configuration/optimization.html>.

[63] Yaniv Leviathan, Matan Kalman, and Yossi Matias. Fast inference from transformers via speculative decoding. In *International Conference on Machine Learning (ICML)*, pages 19274–19286. PMLR, 2023.

[64] Jay Shah, Ganesh Bikshandri, Ying Zhang, Vijay Thakkar, Pradeep Ramani, and Tri Dao. Flashattention-3: Fast and accurate attention with asynchrony and low-precision. *Advances in Neural Information Processing Systems (NeurIPS)*, 37:68658–68685, 2024.

[65] vLLM. vLLM Quantized KV Cache . https://docs.vllm.ai/en/stable/features/quantization/quantized_kvcache.html.

[66] vLLM. vLLM Automatic Prefix Caching . https://docs.vllm.ai/en/latest/features/automatic_prefix_caching.html.

[67] Hongming Zhang and Tianyang Yu. *AlphaZero. Deep Reinforcement Learning: Fundamentals, Research and Applications*, pages 391–415, 2020.

[68] Samy Badreddine, Artur d’Avila Garcez, Luciano Serafini, and Michael Spranger. Logic tensor networks. *Artificial Intelligence*, 303:103649, 2022.

[69] Patrick Hohenecker and Thomas Lukas. Ontology reasoning with deep neural networks. *Journal of Artificial Intelligence Research*, 68:503–540, 2020.

[70] Honghua Dong, Jiayuan Mao, Tian Lin, Chong Wang, Lihong Li, and Denny Zhou. Neural logic machines. In *International Conference on Learning Representations (ICLR)*, 2019.

[71] Connor Pryor, Charles Dickens, Eriq Augustine, Alon Albalak, William Wang, and Lise Getoor. Neupsl: Neural probabilistic soft logic. *Proceedings of the Thirty-Second International Joint Conference on Artificial Intelligence (IJCAI)*, 461:4145–4153, 2022.

[72] Robin Manhaeve, Sebastian Dumančić, Angelika Kimmig, Thomas Demeester, and Luc De Raedt. Neural probabilistic logic programming in deepproblog. *Artificial Intelligence*, 298:103504, 2021.

[73] Zhun Yang, Adam Ishay, and Joohyung Lee. Neurasp: Embracing neural networks into answer set programming. In *29th International Joint Conference on Artificial Intelligence (IJCAI 2020)*, 2020.

[74] Jiayuan Mao, Joshua B Tenenbaum, and Jiajun Wu. Neuro-symbolic concepts. *arXiv preprint arXiv:2505.06191*, 2025.

[75] Joy Hsu, Jiayuan Mao, and Jiajun Wu. Ns3d: Neuro-symbolic grounding of 3d objects and relations. In *Proceedings of the IEEE/CVF Conference on Computer Vision and Pattern Recognition (CVPR)*, pages 2614–2623, 2023.

[76] Robin Manhaeve, Sebastijan Dumancic, Angelika Kimmig, Thomas Demeester, and Luc De Raedt. Deepproblog: Neural probabilistic logic programming. *Advances in neural information processing systems (NeurIPS)*, 31, 2018.

[77] Kevin Ellis, Lionel Wong, Maxwell Nye, Mathias Sable-Meyer, Luc Cary, Lore Anaya Pozo, Luke Hewitt, Armando Solar-Lezama, and Joshua B Tenenbaum. Dreamcoder: growing generalizable, interpretable

knowledge with wake–sleep bayesian program learning. *Philosophical Transactions of the Royal Society A*, 381(2251):20220050, 2023.

[78] Ziyang Li, Jiani Huang, and Mayur Naik. Scallop: A language for neurosymbolic programming. *Proceedings of the ACM on Programming Languages*, 7(PLDI):1463–1487, 2023.

[79] Zishen Wan, Che-Kai Liu, Hanchen Yang, Ritik Raj, Chaojian Li, Haoran You, Yonggan Fu, Cheng Wan, Ananda Samajdar, Yingyan Celine Lin, et al. Towards cognitive ai systems: Workload and characterization of neuro-symbolic ai. In *2024 IEEE International Symposium on Performance Analysis of Systems and Software (ISPASS)*, pages 268–279. IEEE, 2024.

[80] Meihua Dang, Anji Liu, and Guy Van den Broeck. Sparse probabilistic circuits via pruning and growing. *Advances in Neural Information Processing Systems (NeurIPS)*, 35:28374–28385, 2022.

[81] Paul Biberstein, Ziyang Li, Joseph Devietti, and Mayur Naik. Lobster: A gpu-accelerated framework for neurosymbolic programming. *arXiv preprint arXiv:2503.21937*, 2025.

[82] Aaditya Naik, Jason Liu, Claire Wang, Amish Sethi, Saikat Dutta, Mayur Naik, and Eric Wong. Dolphin: A programmable framework for scalable neurosymbolic learning. *arXiv preprint arXiv:2410.03348*, 2024.

[83] Jaron Maene, Vincent Derkinderen, and Pedro Zuidberg Dos Martires. Klay: Accelerating arithmetic circuits for neurosymbolic ai. *arXiv preprint arXiv:2410.11415*, 2024.

[84] Zishen Wan, Hanchen Yang, Ritik Raj, Che-Kai Liu, Ananda Samajdar, Arijit Raychowdhury, and Tushar Krishna. Cogsys: Efficient and scalable neurosymbolic cognition system via algorithm-hardware co-design. In *2025 IEEE International Symposium on High Performance Computer Architecture (HPCA)*, pages 775–789. IEEE, 2025.

[85] Zishen Wan, Che-Kai Liu, Hanchen Yang, Ritik Raj, Chaojian Li, Haoran You, Yonggan Fu, Cheng Wan, Sixu Li, Youbin Kim, et al. Towards efficient neuro-symbolic ai: From workload characterization to hardware architecture. *IEEE Transactions on Circuits and Systems for Artificial Intelligence (TCASAI)*, 2024.

[86] Hanchen Yang, Zishen Wan, Ritik Raj, Joongun Park, Ziwei Li, Ananda Samajdar, Arijit Raychowdhury, and Tushar Krishna. Nsflow: An end-to-end fpga framework with scalable dataflow architecture for neuro-symbolic ai. In *2025 62nd ACM/IEEE Design Automation Conference (DAC)*, pages 1–7, 2025.